Journal Pre-proof

Impact of polymer chemistry on critical quality attributes of selective laser sintering 3D printed solid oral dosage forms

Tikhomirov Evgenii, Levine Valerie, Åhlén Michelle, Di Gallo Nicole, Strømme Maria, Kipping Thomas, Quodbach Julian, Lindh Jonas

Please cite this article as: T. Evgenii, L. Valerie, Å. Michelle, et al., Impact of polymer chemistry on critical quality attributes of selective laser sintering 3D printed solid oral dosage forms, (2023), https://doi.org/10.1016/j.ijpx.2023.100203

Impact of Polymer Chemistry on Critical Quality Attributes of Selective Laser Sintering 3D Printed Solid Oral Dosage Forms

Tikhomirov, Evgenii[1], Levine, Valerie[1], Åhlén, Michelle[1], Di Gallo, Nicole[2], Strømme, Maria[1], Kipping, Thomas[2], Quodbach, Julian[3,*], Lindh, Jonas[1,*]

[1]Division of Nanotechnology and Functional Materials, Department of Materials Science and Engineering, Ångström Laboratory, Uppsala University, Uppsala SE-751 03, Box 35, Sweden.

[2]Merck KGaA, Frankfurter Str. 250, Postcode: D033/001, Darmstadt DE-642 93, Germany.

[3]Division of Pharmaceutics, Utrecht Institute for Pharmaceutical Sciences, Utrecht University, Universiteitsweg 99, 3584 CG Utrecht, The Netherlands

Corresponding authors: Jonas Lindh Jonas.Lindh@angstrom.uu.se, Julian Quodbach j.h.j.quodbach@uu.nl

Key words: Additive manufacturing, Three-dimensional printing, Selective laser sintering, Personalized medicines, Drug manufacturing

Abstract

The aim of this study is to investigate the influence of polymer chemistry on the properties of oral dosage forms produced using selective laser sintering (SLS). The dosage forms were printed using different grades of polyvinyl alcohol or copovidone in combination with indomethacin as the active pharmaceutical ingredient. The properties of the printed structures were assessed according to European Pharmacopoeia guidelines at different printing temperatures and laser scanning speeds in order to determine the suitable printing parameters.

The results of the study indicate that the chemical properties of the polymers, such as dynamic viscosity, degree of hydrolyzation, and molecular weight, have significant impact on drug release and kinetics. Drug release rate and supersaturation can be modulated by selecting the appropriate polymer type. Furthermore, the physical properties of the dosage forms printed under the same settings are influenced by the selected polymer type, which determines the ideal manufacturing settings.

This study demonstrates how the chemical properties of the polymer can determine the appropriate choice of manufacturing settings and the final properties of oral dosage forms produced using SLS.

1

1. Introduction

Manipulation of oral dosage forms is often required, particularly within the pediatric population, as well as within groups of patients that suffer from dysphagia or other common comorbidities.[1] In pediatrics, medications are frequently given as "off-label," since they are intended for, authorized, and approved for the adult population.[2,3] Manipulation of dosages is often performed by hand, with a kitchen knife, tablet splitter, or by dispersing the tablets in water and administering a portion of the liquid suspension to the patient.[4] Dividing medications in inaccurate ways can lead to misdosing[5]. This can have extremely serious consequences for the patients in question, as an incorrect dose of a drug, whether too high or too low, can pose a danger to the health and safety of the patient. Since manipulations are not performed with assured reproducibility, each manipulation could contain a different amount of active pharmaceutical ingredient (API), meaning the consequences of each manipulation are largely unknown.[6] A potential solution to this problem is to create personalized medications for patient groups requiring such by the use of additive manufacturing (AM). This technology allows for the selection of the dose, size, and shape, and with this also the dissolution profile, of each oral dosage form.[7]

AM in pharmaceutical research, while relatively new, has been making great advances in recent years. One such type of AM is Fused Deposition Modelling (FDM), which has been intensively researched within pharmaceutical applications since the first publication describing it in 2014.[8,9] Powder printing methods have also gained popularity in recent years, with the creation of Spritam®, the first commercial medication to utilize AM with FDA approval. This medication is produced with a specialized binder jetting (BJ) technology, called ZipDose® technology.[8] BJ is an AM technology in which a binder liquid is selectively dropped onto a powder bed to bind together the powder in a layer-by-layer fashion until a desired object is subsequently created.[10] Some advantages of this technique, in addition to being an FDA-approved commercial process, include that the object printed remains submerged in powder during the print, negating the need for support structures and allowing for more complex geometries. In addition, it is a powder-based process, giving the final object the look of a powder-based tablet, which is a more traditional look shared by tablets produced via the commonly used powder pressing methods. Additionally, there is potential for powder recycling.[11,12] This method, however, often requires post-processing to remove residual solvents and improve the strength of the print.[13] Two different formulations must be developed as well; one for the ink and one for the powder.[14] Additionally, friability of tablets created with this print method is still in the improvement phase, and tablets are more sensitive regarding mechanical properties.[11,15]

Selective Laser Sintering (SLS) has several advantages shared by BJ, but does not share the potential disadvantages of dual formulation development or post-processing beyond dusting off the printed objects. SLS was first introduced in 1989 by Carl. R. Deckard,[16] and is a type of powder bed fusion technique in which a powder material is fused together by a laser in a layer-by-layer fashion. The object printed remains fully immersed in powder material as it is printed, causing no need for support materials and

allowing for more complex geometries and structures, as well as possible high resolution, and the potential for some powder recycling. These possible advantages are also shared with other powder-processing methods, such as BJ. A disadvantage of SLS, however, is that it is performed at relatively high temperatures, which could potentially cause degradation to the API present in the formulation.[17] While the laser energy is mostly converted to thermal energy, this laser beam energy may additionally impact the molecular integrity of the drug substance. SLS, as with the other AM methods, was not designed with pharmaceutical development specifically in mind. Originally, powder-based processes were developed to create plastic prototypes, then evolved to metal[18–20] and ceramic powders.[21,22] Over time, the applications and material range of powder-based AM expanded further and further, encompassing even pharmaceutical materials and applications.[10,23–26]

As the applicability of SLS for pharmaceutical applications increased, with the first publications in this field in 2017[17] and the number expanding each year, with Scopus showing 38 new publications in the years 2021 and 2022, certain polymers for pharmaceutical application were frequently used. However, none of these polymers were specifically designed for use in an SLS printer. Due to the nature of SLS, the conditions the polymers meet during production of oral dosage forms are different than in traditional production methods. The polymers face elevated temperatures from both the sintering process and the heated chamber and chamber elements of the printer. Polymer materials designed for hot melt extrusion (HME)[27–29] were a logical choice for use in this study, as hot-melt extrusion also exposes the materials involved to increased temperatures of 100-150 °C.[30]

The polymer polyvinyl alcohol (PVA, Figure 1), sold under the commercial name Parteck® MXP 4-88, is a polymer often used as a pharmaceutical excipient for HME.[31,32] At this time, the authors are aware of only one publication involving the creation of oral dosage forms using SLS with PVA.[33] PVA has a high degradation temperature (above 200 °C)[34] and is already being used for HME, and is therefore of interest for application with SLS for oral dosage forms.

PVP-VA (1) and PVP-VA (2) (copolymer of 1-vinyl-2-pyrrolidone and vinyl acetate, Figure 1), respectively known commercially as Kollidon ® VA 64 and Plasdone™ S630, also have many of the same positive characteristics as PVA. PVP-VA (1) is designed commercially to be used as a dry binder in tablets or as a matrix former for amorphous solid dispersions.[35] However, it has gained popularity for use in SLS, with seven out of 15 papers published as of 2020 on the topic of SLS for solid oral dosage forms utilizing this polymer.[25,36] PVP-VA (1) is suited for SLS due to the low glass transition temperature, T_g, of the material, which allows for lower processing temperatures of the material. Additionally, it allows for quickly disintegrating dosage forms, a result of the erodible instant release matrix.[37]

The new-to-market PVA-based polymer PVA 3-82, commercially Parteck® MXP 3-82, and a technical development grade PVA 5-74 are also designed for use in HME. These materials could potentially find applications in SLS, since many polymers designed for HME have been successfully repurposed.
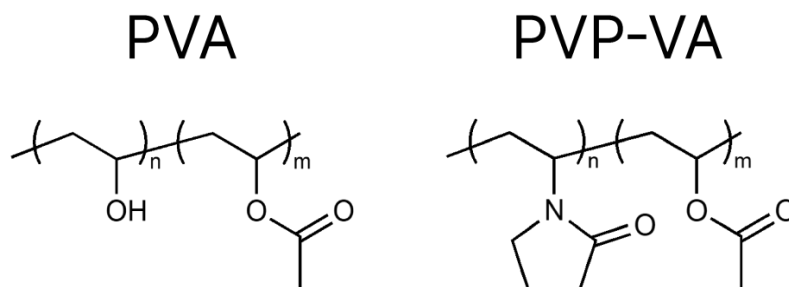
Figure 1. Chemical structures of PVA and PVP-VA.

For the continued development and adoption of SLS as a means to produce oral dosage forms, understanding the impact of polymer types and grades is of high importance. It is additionally paramount to examine the printer settings impact on the different polymer types and grades for developing better printing parameters. Therefore, the polymers PVA 4-88, PVA 3-82, PVA 5-74, PVP-VA (1), and PVP-VA (2) were analyzed using different print temperatures and laser scan speeds, with these materials falling under the category of being PVA-based or PVP-VA-based materials. The inclusion of different PVA grades with different degrees of modification is especially interesting, as it allows a direct comparison of the influence of polymer chemistry as well as process settings on the process and product quality. The first number in the name of PVA grades represents the viscosity of 4% PVA solution in water at 20 ˚C in mPa·s, while the second number indicates how many acetate groups were hydrolyzed (molar %) from the starting polymer polyvinyl acetate. The more hydrolyzed acetate groups, the lower the hydrophobicity of the polymer. Meanwhile, PVP-VA grades have different molecular weight (or degree of polymerization) expressed in K-value calculated from the kinematic viscosity of a 1% aqueous solution. The K-values of PVP-VA (1) and PVP-VA (2) are in the range of 25.2 – 30.8 and 25.4 – 34.2, respectively. Analyses were conducted on the resultant tablets, adhering as closely as possible to European Pharmacopoeia (Ph. Eur.)[38] guidelines for conventional uncoated tablets.

In this study, it was imperative to study the chemistry of the chosen polymers and how this impacts the overall properties of the resultant dosage forms. Additionally, this study aims to investigate the dissolution profiles of the resultant dosage forms depending on the implementation of different polymers and print conditions. To gain insight into the results obtained from this study, the pure polymers were first investigated. To interpret the results in a broader context, a principal component analysis (PCA) was used, as well as drug content tests of the resultant tablets and API dissolution tests. The results will lead to a better understanding of these materials and a guidance for appropriate print conditions of the selected polymers to achieve desired print results with respect to oral dosage forms.

2. Materials and methods

2.1. Materials

4

Indomethacin was produced by Tokyo Chemical Industry Co., LTD (6-15-19, Toshima, Kitaku, Tokyo, Japan) and provided by Merck KGaA (Darmstadt, Germany). Silica based effect pigment (Candurin ® NXT Ruby Red), silicon dioxide colloidal (EMPROVE® ESSENTIAL, Ph. Eur., JP, NF, E 551), P1 (Parteck® MXP, PVA 3-82), P2 (PVA 5-74), and P3 (Parteck® MXP, PVA-4-88) were kindly provided by Merck KGaA (Darmstadt, Germany). P4 (Kollidon ® VA 64, copovidone) was kindly provided by BASF SE (Ludwigshafen, Germany). P5 (Plasdone™ S-630, copovidone) was kindly provided by Ashland Industries Europe GmbH (Schaffhausen, Switzerland).

2.2. *Formulation preparation*

All excipients were weighed, manually mixed, and sieved using a 315 µm stainless-steel test sieve (VWR International AB, Stockholm, Sweden). The sieved formulations were mixed again using a Turbula shaker (Turbula T2F shaker, Glen Mills, Inc., Clifton, NJ, US) for 20 min. Pigment and colloidal silica were added to the formulations to enhance the laser energy absorption of the powders and to improve powder flowability during the layer application process, respectively. Then, the mixed powder was heat-treated at 70 ˚C in an oven (Incucell®, BMT Medical Technology s. r. o., Brno, Czech Republic) overnight to remove any moisture that may have been absorbed by the formulation. Then, the powder was mixed again using a Turbula shaker. The formulations were prepared in large enough volumes (approx. 1500 mL) to provide materials for several print batches. Each formulation consists of 1 wt% of pigment, 10 wt% of indomethacin, 0.5 wt% of silicon dioxide, and 88.5 wt% of polymer. Since all formulations have the same content, except for the polymer, their names were compiled as follows - FP1. Where "F" stands for "formulation" and P1 is the name of the polymer.

2.3. *Selective laser sintering (SLS) of dosage forms*

The tablet model (Figure 2) was created in Fusion 360 (Autodesk, USA) and subsequently uploaded as an STL-file to Sintratec Central 1.2.7 (Sintratec AG, Brugg, Switzerland). A batch of 36 tablets was created and arranged at the center of the print bed and the following parameters were used for all formulations: 50 µm perimeter offset, 50 µm hatching space, 150 µm hatching offset, and three perimeter paths.
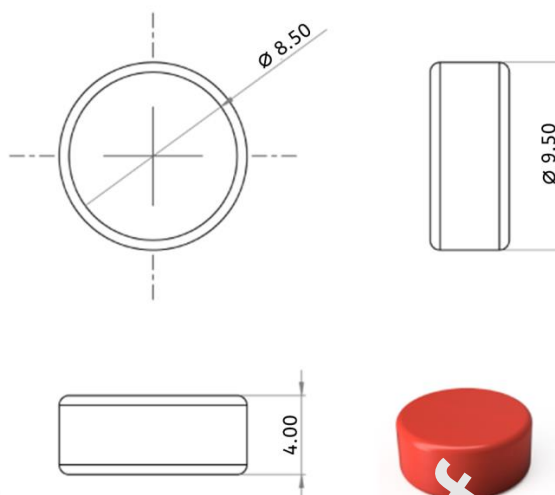
Figure 2. Orthographic projection and a 3D model of the dosage form. All dimensions are in mm.

The prepared formulation was loaded into the feeding compartment of a Sintratec Kit SLS 3D printer (Sintratec AG, Brugg, Switzerland). A thin layer of powder was then spread upon the build platform after which the powder beds were slowly heated to the printing and standby temperatures. The sintering was carried out using a 2.3 W diode laser (λ = 455 nm) in accordance with the template models given in the STL-file in a layer-by-layer fashion. The modeled tablets were printed flat to the build platform, using a layer height of 125 μm for all polymers. Specific values for the laser scanning speed (200, 300 and 400 mm/s) were chosen when printing the different batches and each speed was used at three different printing temperatures. The finished batches were collected from the build platform at the end of the printing process by sieving. The tablets were additionally de-dusted using pressurized air to remove excess powder and stored in sealed containers for further analysis at room temperature. The storage time between printing and analysis did not exceed two weeks. This relatively short duration was chosen to minimize any potential API recrystallisation or changes in the printed samples over time. Names of the tablet batches were given after the combination of these two parameters used during the printing process. For example, FP1-75-200: FP1 – the name of the formulation, 75 – temperature in degrees Celsius of the printing bed, 200 – scanning speed of the laser in mm/s.

2.4.   *Characterization*

Powder X-ray diffraction (PXRD) diffractograms of the pristine and heat-treated powder formulations as well as the printed dosage forms were collected on a D8 Advance TwinTwin X-ray diffractometer (Bruker AXS GmbH, Bremen, Germany) using Cu-K$\alpha_{1,2}$ (λ = 1.5418 Å) radiation. The instrument was operated at 40 mA and 40 kV, using

a step-size of 0.02˚. Differential scanning calorimetry (DSC) thermograms were obtained on a Mettler Toledo DSC 3+ (Schwerzenbach, Switzerland) using a heating and cooling rate of 10 ˚C min^{-1} and nitrogen as purge gas. Repeated heating-cooling measurements were carried out from -40 to 200 ˚C and from 200 to 10 ˚C in the first cycle, and from 10 to 200 ˚C in the following cycles. The dimensions (n = 10) and weights (n = 36) of the printed tablet were examined using a digital caliper and an analytical balance (Mettler Toledo XS 64 Analytical Balance, Schwerzenbach, Switzerland). Friability tests were carried out in accordance with the 10th edition of Ph. Eur. on approx. 6.5 g of tablets using a Pharmatest PTF E friabilator (Hainberg, Germany) at 25 rpm and for 100 rotations. The tablets were carefully weighed pre- and post-rotation and total mass loss of the tablets (i.e., friability) was calculated. The particle size measurement was performed using a Mastersizer 3000 (Malvern Panalytical Ltd, Malvern, United Kingdom) using ten measurements for each sample with 10 s measurement duration and the results are presented as volume-based.

2.5. *Dissolution test*

Dissolution tests were carried out using a Sotax AT7 Smart Dissolution USP type II Tester (Aesch, Switzerland). *In-vitro* drug release profiles for the 3D printed tablets (n = 3) were performed in 500 mL of Simulated Gastric Fluid (SGF; 800 ml 1M HCl, 20 g NaCl ad 10L, pH 1.2) at 37 ± 0.5 ˚C and 50 rpm using a sinker to weigh down the tablets. The drug concentration in the dissolution media was determined with high performance liquid chromatography (HPLC) (Agilent 1260 Infinity II, Agilent Technologies, Inc., Santa Clara, USA) on 10 μL of filtered sample (0.45 μm PTFE filters, VWR International GmbH). The HPLC assays were performed using a mobile phase composition of acetonitrile and phosphate buffer (0,01M NaH$_2$PO*H$_2$O 1.38g/L+ 0.01M Na$_2$HPO$_4$ 1.41g/L) in 1 to 1 ratio. Samples were injected into a Supelcosil LC-18 column (30 x 4 mm, 5μm) at a flowrate of 1 mL min^{-1} and at 40 ˚C and the eluent analyzed at 254 nm.

2.6. *Drug content*

The drug content of 3D printed tablets (n = 5) was evaluated by placing the individually pre-weighed tablets in 100 mL volumetric flasks containing 50 mL Milli-Q water. The tablets were stirred at 40 ˚C and 500 rpm for 1 h, after which the solutions were diluted with 50 mL HPLC mobile phase, stirred again for 30 min, cooled down to room temperature and filled up to 100 mL with mobile phase. Then, 5 mL of substance was filtered (0.45 μm PTFE filters, VWR International GmbH) and analyzed using the same HPLC method as described above.

2.7. *Statistics methods*

The PCA and two-factor analysis of variance (ANOVA) were carried out to analyze the multi-dimensional dataset and defines the significance of difference. Both methods were performed using RStudio (Posit Software, Boston, USA).

3. Results and discussions

The impact of polymer chemistry on the properties of printed dosage forms was thoroughly investigated through a series of experiments. These experiments involved adjusting printing parameters such as laser scanning speed and printing temperature. The objective was to determine the suitable printing conditions for each selected polymer, aiming to achieve dosage form characteristics that closely align with the requirements specified in the Ph. Eur. Furthermore, the printed dosage forms can be categorized as solid dispersions (SD), leading to an exploration of how the choice of polymer affects API solubility.

3.1. Pure polymers characterization

The polymer particle size distribution defines what layer height can be used for a successful print. If the average particle size is bigger than the layer height, it will lead to the powder dragging and, consequently, shifting of layers. However, if the layer height is too large, the heat energy will not be sufficient to sinter the whole layer thickness and provide enough interaction between layers, resulting in delamination. According to Table 1, the x50 value varies from 33.4 to 102.0 μm for the different polymers. The layer height of 125 μm was selected for all polymers.

Table 1. Polymers particle size distribution represented as percentiles (n=10, mean ± sd).

Polymer	x10 / μm	x50 / μm	x90 / μm
P1	20.1±0.4	79.8±2.2	197.0±14.2
P2	26.4±0.7	102.0±1.9	249.0±7.6
P3	11.8±0.26	40.0±0.9	100.0±11.7
P4	27.5±0.9	76.7±1.6	141.0±5.8
P5	17.1±0.1	65.4±1.1	137.0±4.5
Indomethacin	7.1±0.3	26.4±0.4	83. ±10.0

The powder mixtures consist of 88.5 wt% of polymer, which works as a binding material for 10 wt% of API. The sintering process can be classified as a "partial melting" because of the vague distinction between the binder and the structural material.[39] Partial melting presumes that only the surfaces of the polymer are molten, which leads to the consolidation of polymer chains. Since this phenomenon is driven by the heat energy

8

transferred from the external heat source, (lamps heating the powder bed and print chamber) and the laser beam, the thermal properties of the polymers have a significant impact on the printability of the API-loaded mixtures.

The T_g of the pure polymers was investigated using DSC and are shown in Figure 3. P3 showed a T_g of 68 °C, which is close to the values obtained for P1 and P2 (64 and 62 °C, respectively). Since the second heating cycle was used for data analysis, the T_g values are increased due to water evaporation in the previous cycle.[40] The T_g of P4 and P5 were also similar, at 109 and 110 °C, respectively. These are both PVP-VA-based polymers, so the similarity is expected, just as the similarity between P1, P2, and P3 is expected since these are all grades of PVA.
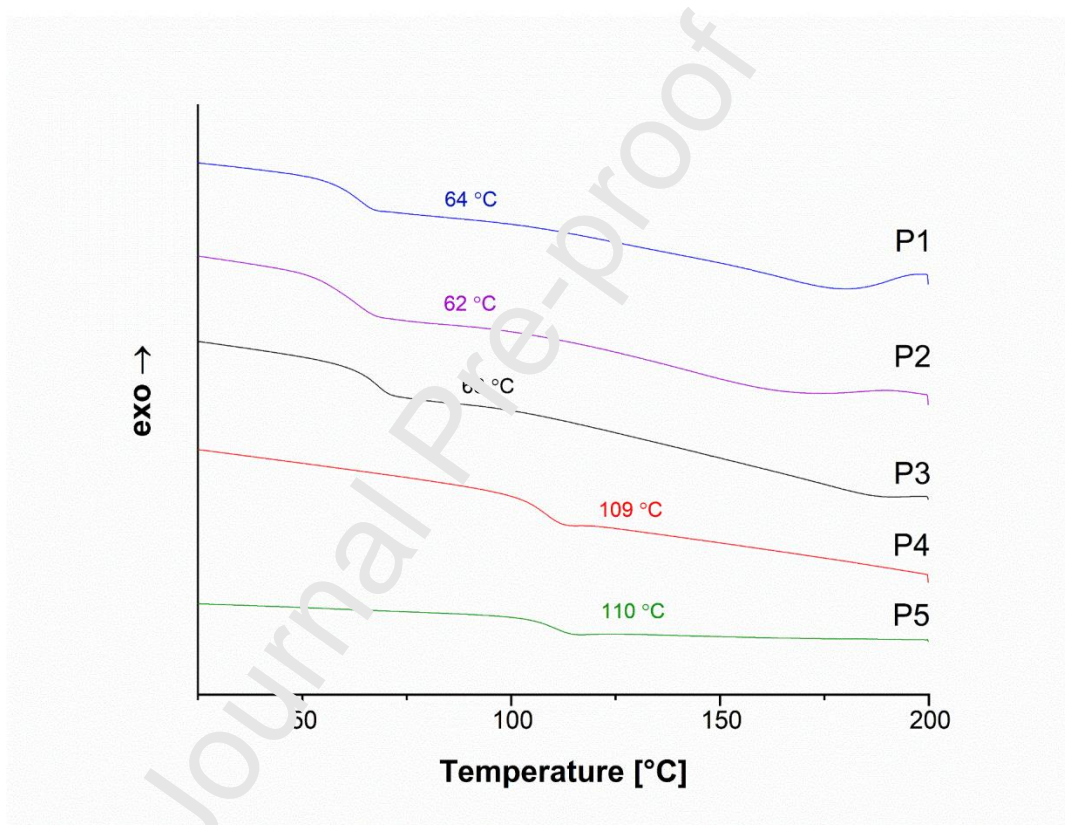

Figure 3. DSC thermograms of the pure polymer powders for PVA-based (P1, P2, P3) and PVP-VA-based (P4, P5) polymers (second heating cycle).

3.2. Characterization of printed dosage forms

3.2.1. PVA-based printed dosage forms

DSC analysis was carried out for all PVA-based dosage forms and formulations. The lack of an endothermal peak associated with the API melting peak was observed (Figure 4 A) for dosage forms printed at the highest temperature and lowest laser scanning speed, 125 °C and 200 mm/s respectively. In contrast, formulations have distinct API endothermal peaks for all PVA-based polymers (Figure 4 B). DSC thermograms of dosage forms (Figure S1, S3, S5) show that the amorphization of API depends on the

type of polymer, and there are no traces of crystalline API endothermal peaks in batches FP3-125-200, FP3-75-200, FP3-100-200, FP3-125-300. The dosage forms printed with P3 (highest degree of hydrolysis among PVA grades with 88% hydrolyzation) showed the best tendency for API amorphization. Four out of nine batches had fully amorphized API. However, when using P1 and P2, all batches except FP1-125-300, FP2-125-200, and FP2-125-300 have small but detectable API endothermal peaks. Moreover, thermograms support the concept that laser scanning speed as well as printing temperature strongly affects the API endothermal peaks. Thus, dosage forms printed at the same temperature showed a larger residual API peak at higher laser scanning speeds. At the same time, comparing the endothermal peak areas (Table 3, 4, 5), the changes in API amorphization level can be estimated for dosage forms printed at different speeds and temperatures. The three PVA grades show different changes in endothermal peak area, depending on their dynamic viscosity. The P1 grade with a viscosity of 3 mPa·s has the smallest change, while the P3 grade with a viscosity of 4 mPa·s shows a moderate change, and the P2 grade with the highest viscosity of 5 mPa·s has the biggest change. For instance, comparing batches printed at the same temperature of 100 °C and increasing the scanning speed from 200 mm/s to 300 mm/s, endothermal peak areas increase by 2.9 mJ, 7.1 mJ, and 3.6 mJ for P1, P2, and P3 respectively. The difference in these values is another indication of the polymer's role in the amorphization of the API.
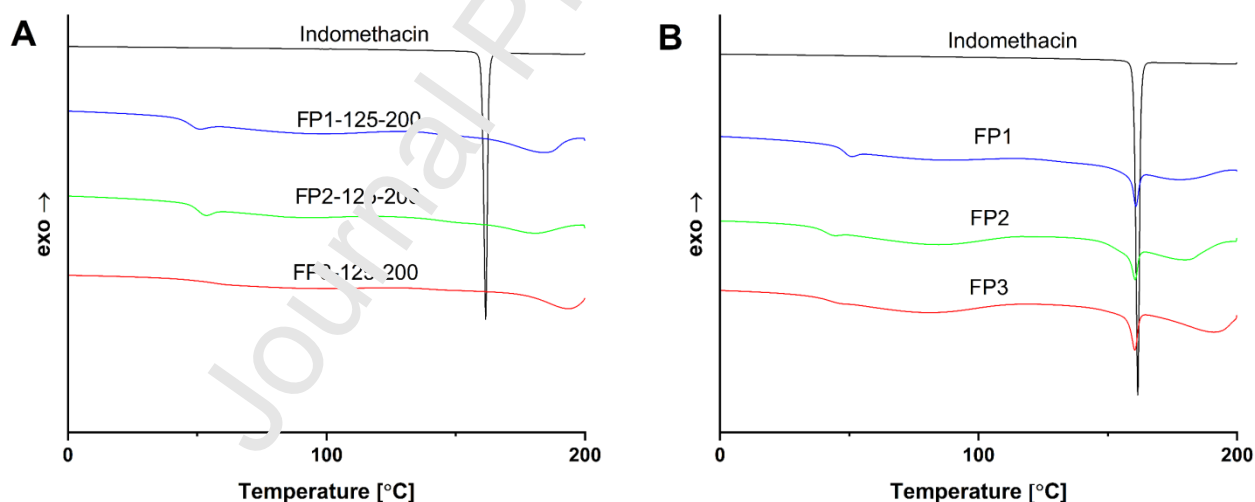

Figure 4. DSC thermograms of the PVA-based dosage forms, physical mixture and API. (A) Dosage forms. (B) Physical mixture, API, and the dosage form with the best print quality.

Additionally, the crystallinity of the API in dosage forms and in the physical mixtures was evaluated by PXRD. According to the PXRD diffractograms of dosage forms (Figure 5), the absence of the API crystallinity peaks was observed for all three PVA-based dosage forms printed at 200 mm/s and 125 ˚C, whereas signals representing crystalline API are clearly visible in the physical mixture samples. However, a few small crystallinity peaks related to unsintered powder residuals may be observed in the

diffractograms of other batches printed at lower temperatures and higher laser scanning speeds. The PXRD diffractograms of all printed dosage forms can be seen in the supplementary materials (Figure S2, S4, S6) which show similarities in API amorphization for all PVA-based polymers. The presence of API crystallinity peaks decreases with decreasing scanning speeds and increasing printing temperatures, i.e. by increasing the energy input. However, the level of amorphization depends on the selected polymer. For instance, the lack of API crystallinity peaks was observed for all batches printed at 200 mm/s and the FP3-125-300 batch for the P3 polymer. Conversely, only batches FP1-125-300, FP2-125-200, and FP2-125-300 showed full API amorphization when using the P1 and P2 polymers. The better API amorphization capability of PVA 4-88 (P3) may be explained by the highest level of hydrolyzation (88 mol%) which provides more locations for hydrogen bonding interactions between the drug and the polymer.

This result corresponds well with the DSC analysis data and indicates successful amorphization of the API in the dosage forms and dependencies between laser scanning speed, printing temperature, and polymer type.
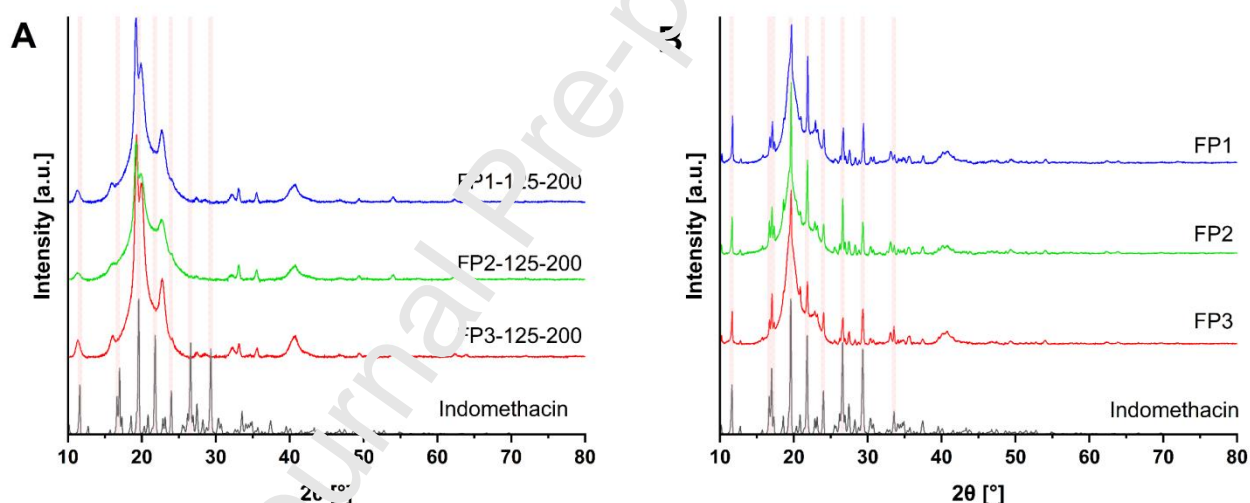

Figure 5. PXRD diffractograms of PVA-based dosage forms, physical mixture and API. (A) Dosage forms and API. (B) Physical mixtures and API.

The average mass of all 36 printed tablets was measured for each set of printing parameters for all polymers (Table S1, S2, S3). According to Ph. Eur. 2.9.5 – Uniformity of Mass of Single-Dose Preparation, no more than two individual tablets may deviate from the average mass by more than a certain percentage. The percentage deviation for tablets with an average mass between 80 and 250 mg is 7.5%. Therefore, only batches FP3-100-200 and FP3-125-200 of polymer P3 fulfilled the mass uniformity requirement with one and two outliers, respectively. However, batches printed with P1 and P2 polymers demonstrated better weight uniformity. All batches printed at 125 °C and FP1-100-200 had one or two outliers for P1. In the case of P2, only the batch printed at 100 °C and 300 mm/s has three outliers while the other batches have one or zero.

11

A two-way ANOVA was conducted to examine the effects of speed (200, 300, 400 mm/s) and temperature (75, 100, 125 ˚C) on the mass of the printed tablets. Since some batches printed at 75 °C were too fragile to handle and carry out any type of measurements on, they were excluded from the examination. Table 2 shows the ANOVA results for each polymer considering speed and temperature as factors and the interaction between them. The statistically significant difference in mean mass by both speed and temperature was observed for all polymers. Moreover, there was a statistically significant interaction between the effects on the mass.

Table 2. ANOVA results for PVA-based dosage forms.

Formulation	Speed		Temperature		Interaction	
	F	p	F	p	F	p
FP1	872.8	<0.001	1023.0	<0.001	15.9	<0.001
FP2	623.3	<0.001	369.4	<0.001	83.7	<0.001
FP3	549.5	<0.001	216.6	<0.001	4.5	0.0045

Additionally, the mass-distribution box-plot is shown in Figure 6 in order to define the dependencies between laser scanning speed, printing speed, and mass of the dosage forms.
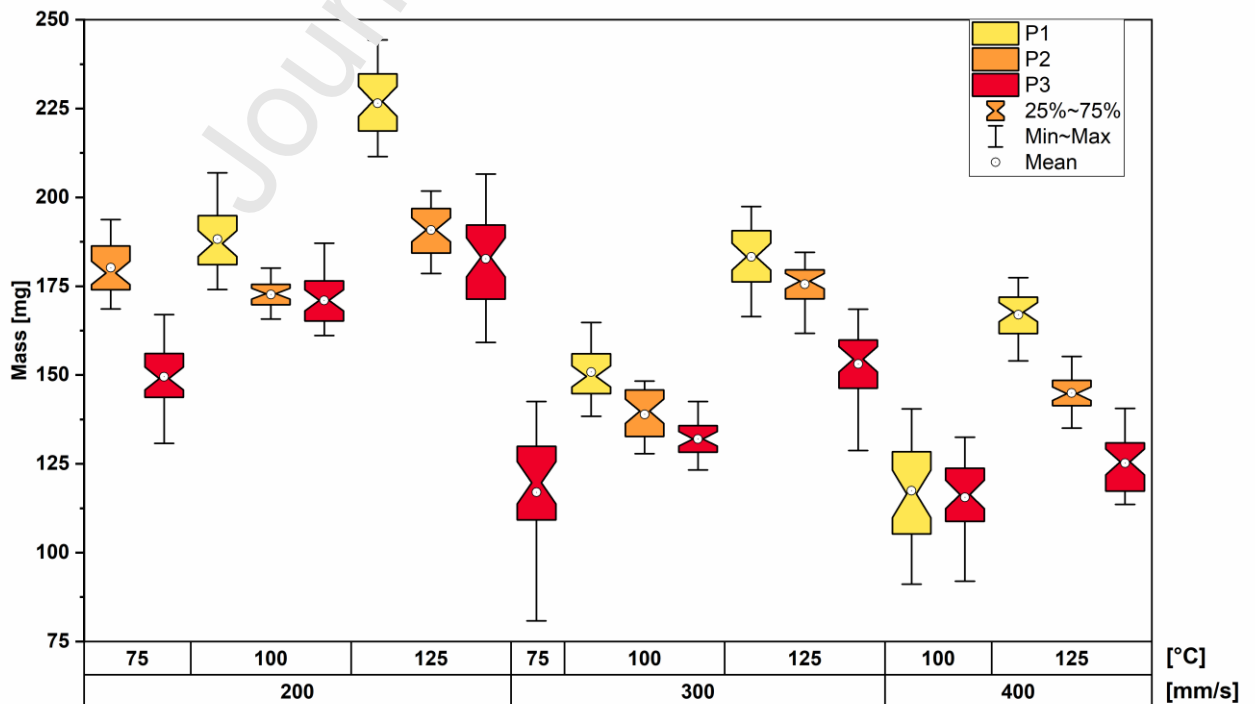
Figure 6. Mass distribution box-plots of PVA-based dosage forms grouped by printing temperature, scanning speed, and polymer type.

It is clear from the graph that the mass of the dosage forms increases with increasing printing temperature and decreasing laser scanning speed in case of P1. However, the higher mass of P2-based dosage forms printed at 200 mm/s and 75 °C than for the dosage forms printed at 100 °C and the same laser scanning speed can be observed (p<0.001, according to a post hoc analysis), while the rest follows the same pattern as for P1. Analyzing mass distribution of P3-based dosage forms, the same dependence as for the P1 polymer is observed, but some batches have mass deviation from the mean value which make the comparison inconsistent. Moreover, the P1-based dosage forms showed tendency to have the greater mass than other grades printed using the same parameters. The mass difference is explained by the density variations of the printed layers depending on the amount of transferred heat energy during the printing.[41]

Friability testing showed that mass losses change depending on the previously discussed parameters; printing temperature, laser scanning speed, and polymer type (Table S1, S2, S3). Some batches produced tablets that were very fragile and those tablets were almost fully destroyed during the testing (FP3-75-200, FP3-100-400, FP3-125-400, FP1-100-400, FP2-75-200, FP2-100-300). Mass losses for the rest of the batches were greater than 1%, which is not acceptable according to Ph. Eur. 2.9.7. Nevertheless, the mass losses steadily decreased with increasing printing temperature and decreasing laser scanning speed. Interestingly, no relationship between employed PVA grade and friability could be established.

The gathered data for all printed PVA-based batches was compiled in tables in the supplementary information section (Table S1, S2, S3). Table 3 shows the results of the best overall performing batches, which have the lowest number of outliers, lowest mass losses, and full API amorphization. It is noticeable that printing parameters for these batches were the same for all three PVA grades, 125 °C printing temperature and 200 mm/s laser scanning speed. These parameters provide the highest energy input which results in better sintering and API amorphization.

Table 3. Characterization of PVA-based dosage forms from the best performing batches.

Batch name	Average mass, mg	N of outliers*	Mass losses, %	API endothermal peak area, mJ
FP1-125-200	226.5 ± 4.1	1	2.3	0
FP2-125-200	190.8 ± 3.3	0	4.5	0
FP3-125-200	180.4 ± 4.6	2	2.0	0

* - Number of tablets that deviate from the average mass by more than 7.5%.

Dosage form weight and uniformity are crucial parameters, as they have a direct impact on the dose of API. The heavier the tablet, the higher the dose of API it contains. Furthermore, the printing conditions impact both the Ph. Eur. requirements and appearance of the tablets. The appearance is a relative value observed empirically and can be described as a combination of visual qualitative properties, e.g., layer lamination, roughness, and shape.

Figure 7 shows a clear difference between dosage forms based on the printing temperature and laser scanning speeds utilized in this study. The dosage forms printed at 75 °C show well-defined layers on the side profile view. Moreover, the dosage forms printed at 75 °C have a shift along the x-y plane and a rough surface. This is due to the low temperature, leading to poorly adhering layers. The shape is also affected, with the samples printed at 75 °C appearing more fragile with more defects and less similar to the tablet model at the outermost edges. At the same time, the dosage form printed at a speed of 400 mm/s has an irregular shape and a pronounced surface roughness, especially in case of P3 where collapsed dosage forms printed at 100 °C are observed. The dosage forms printed at a temperature of 125 °C and a scanning speed of 200 and 300 mm/s have the high resemblance to the model's cylindrical shape without any defects for any of the three polymers.
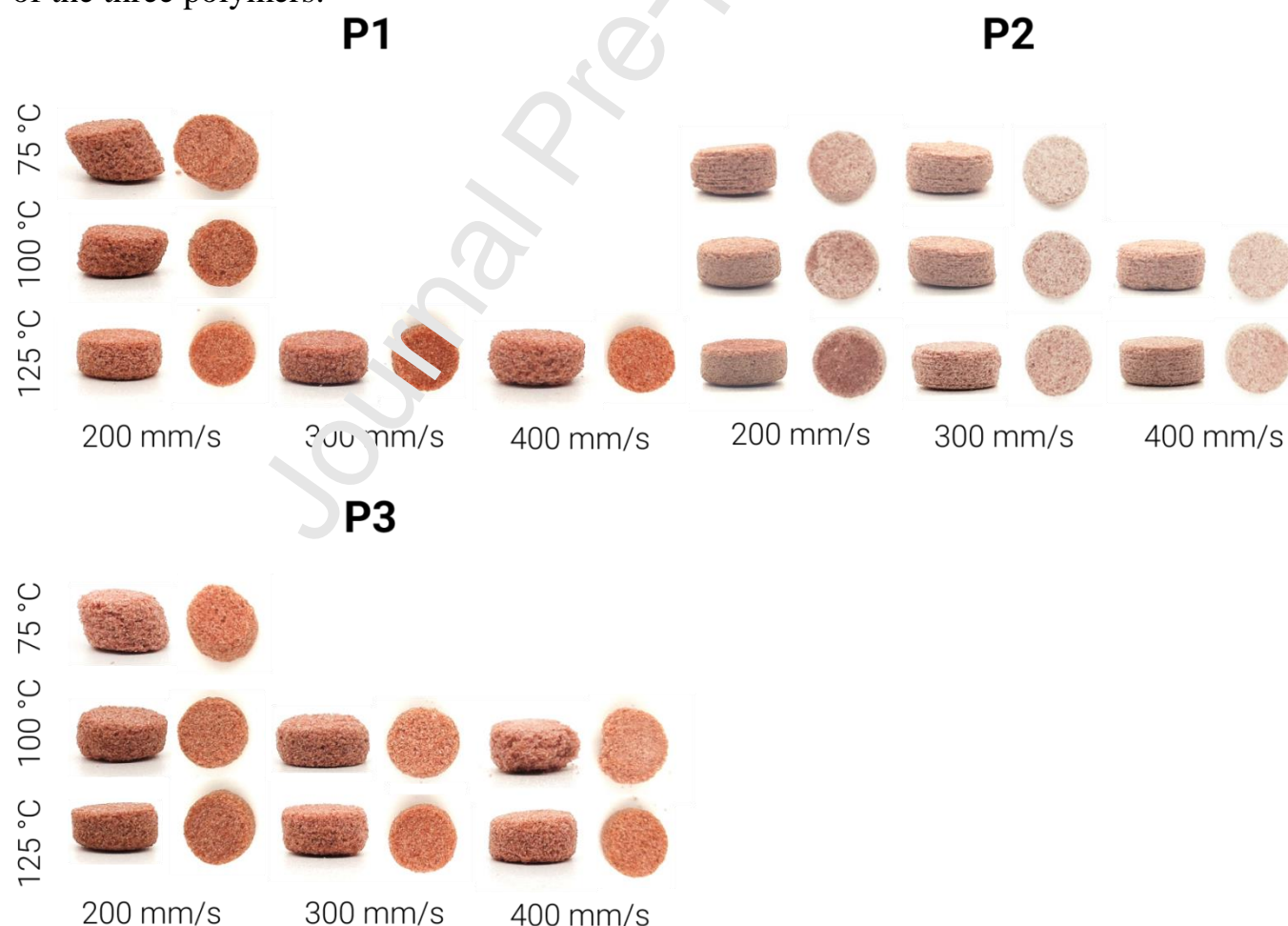

Figure 7. Camera images of PVA-based dosage forms printed at different speeds and temperatures.

The tablets were impacted by the laser scan speed, with a higher degree of sintering visible at the lower laser scan speeds. As seen in Figure 7, the color of the tablets is lighter at higher laser scanning speeds and darker at lower laser scanning speeds, as a denser and more well sintered tablet will have a darker color. The density of printed structures can be estimated by calculating the ratio between the mass and volume of the structure. In the case where all printed structures are produced using the same printing model and thus have the same volume, a higher mass indicates a higher density.

3.2.2. PVP-VA-based printed dosage forms

The printing settings were changed for the PVP-VA based mixtures. The tablets printed at temperatures higher than 112.5 °C were fused together with the surrounding powder, which made it impossible to run characterization experiments. Furthermore, the lower temperature limit of 75 °C was only successful at a speed of 200 mm/s for the P4 polymer-based formulation. Otherwise, the printed structures were too fragile to handle. Consequently, PVP-VA – based mixtures had a more limited printing temperature range for successful prints.

According to the DSC results (Figure S7, S9), there were no visible peaks indicating the presence of crystalline API for the majority of the tablets, with the exception of FP4-100-400, FP4-112.5-400, and FP5-100-400, FP5-112.5-400. These were printed at the highest scanning speed, which allows the least amount of energy input in the tablets, so the presence of some crystalline API traces in these samples is explained by the low laser energy input. The decrease of peak intensities representing crystalline API was already visible in the heat-treated powder formulation. When comparing the best overall sample (Figure 8) based on the test prints for these polymers, FP4-112.5-200 and FP5-112.5-200, with the powder mixture and pure API, the API peak is not present in either. The heat treatment of the powder mixture already mitigated this peak in the powder mixture.
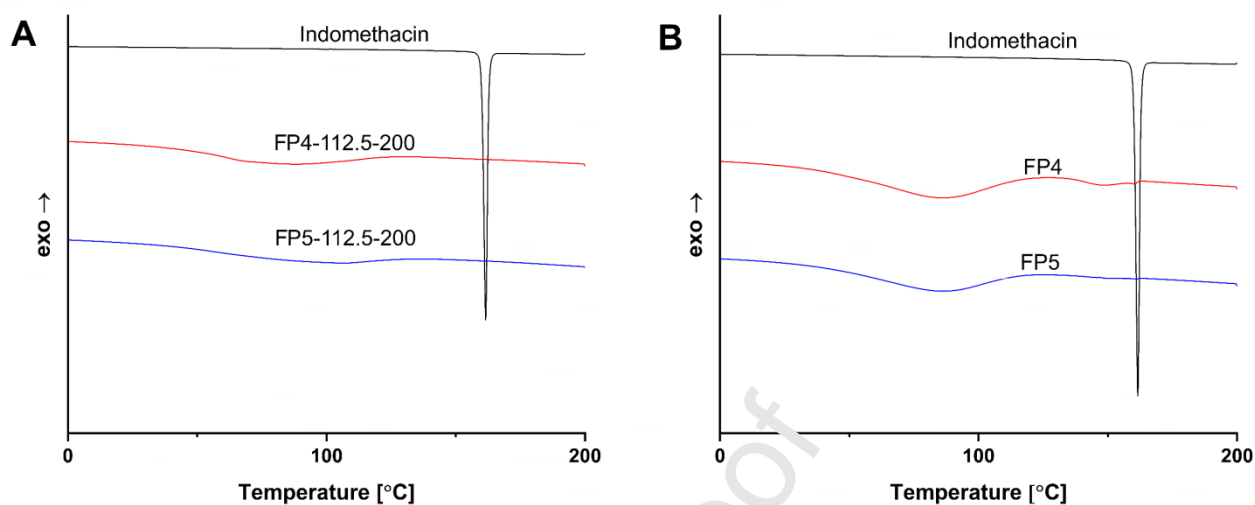
Figure 8. DSC thermograms of the PVP-VA-based dosage forms, physical mixture and API. (A) Dosage forms. (B) Physical mixture, API, and the dosage form with the best print quality.

In contrast, PXRD diffractograms (Figure S8, S10) show crystalline API presence in the formulation and all printed structures. The peaks intensity decreases in the same manner as for dosage forms printed using PVA-based formulations. Even though the peaks intensity decreases with increasing temperature and decreasing laser scanning speed, it cannot be claimed that full API amorphization was achieved for the PVP-VA-based dosage forms even for the batches printed at a lower laser scanning speed of 200 mm/s and the highest temperature of 112.5 °C (Figure 9). The contradiction in two different approaches, DSC and PXRD, shows that DSC cannot be used reliably for crystalline API detection alone.
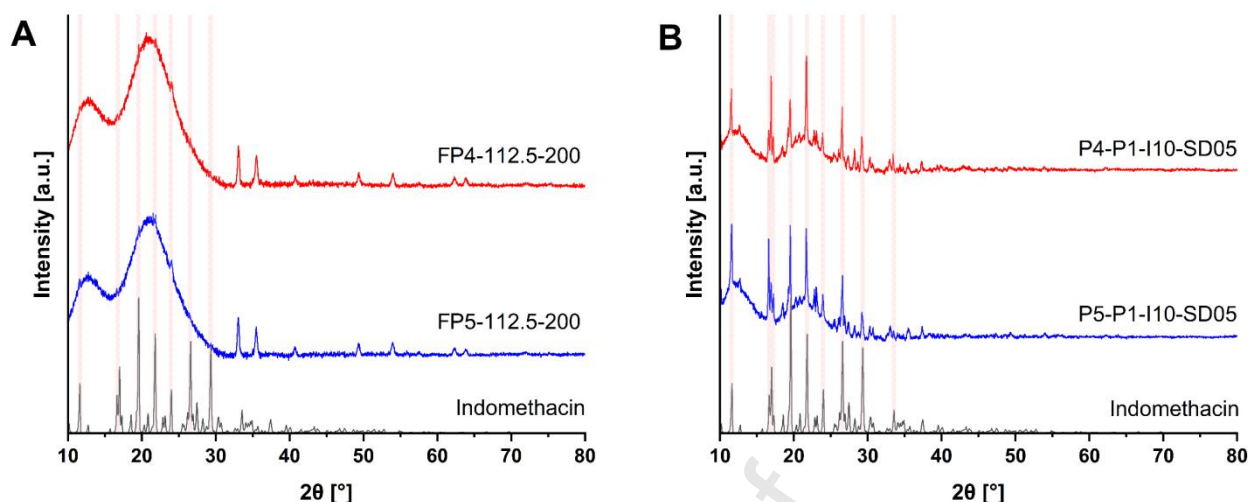
Figure 9. PXRD diffractograms of PVP-VA-based dosage forms, physical mixture and API. (A) Dosage forms and API. (B) Physical mixture, API and the dosage form with the best print quality.

The average mass of the tablets for each set of parameters was measured in the same manner as for the PVA-based polymers. According to Table S4, only the batch printed at a laser scanning speed of 200 mm/s and at a temperature of 100 °C does not have any outliers in the case of P4. Whereas, for P5 (Table S5), the batch with the least number of outliers, two, was printed at 200 mm/s and a temperature of 112.5 °C. The rest of the batches have three or more outliers out of 36 printed tablets.

Again, a two-way ANOVA was conducted to examine the effects of laser scanning speed (200, 300, 400 mm/s) and temperature (100, 112.5 °C) on the mass of the printed tablets. The batch printed at a temperature of 75 °C was not considered in the statistical analysis.

Table 4. ANOVA results for PVP-VA-based dosage forms.

Formulation	Speed		Temperature		Interaction	
	F	p	F	p	F	p
FP4	876.1	<0.001	348.65	<0.001	26.49	<0.001
FP5	635.5	<0.001	67.8	<0.001	9.0	<0.001

The mass distribution boxplot reveals the same dependencies as for PVA-based polymers. The average mass increases when lowering laser scanning speeds and increasing printing temperatures. Moreover, the dosage forms printed with P4 are more sensitive to changes in chamber temperature than the dosage forms printed with P5. This

is especially pronounced at a print speed of 300 mm/s where the median mass differences between dosage forms printed at the two different temperatures are 32.2 mg and 3.0 mg for P4 and P5, respectively.
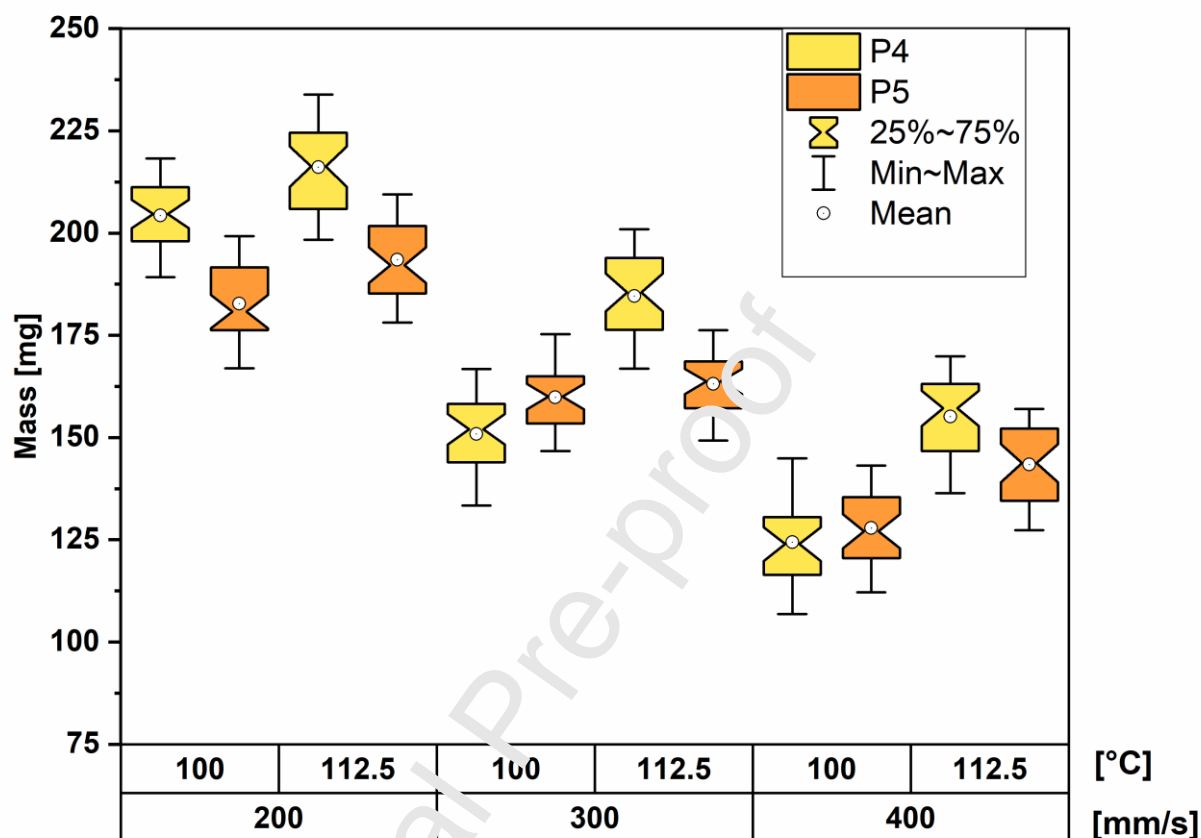

Figure 10. Mass distribution box-plots grouped by printing temperature and scanning speed.

The friability test results for PVP-VA-based dosage forms indicate the speed and temperature dependence, similar to the PVA-based dosage forms. According to Table S4 and S5, mass losses decrease with increasing temperatures and lower scanning speeds. Tablets of both batches printed at a speed of 400 mm/s disintegrated for P4 and P5 polymers. Moreover, P5 showed worse friability performance, with only the batch FP5-100-200 surviving friability testing among all batches printed at a temperature of 100 °C. Overall, none of batches fulfilled the Ph.Eur. requirements for conventional uncoated tablets. The endothermic peak area was much lower than for the previous polymer and could only be measured for batches FP4-100-300 and FP4-100-400. However, due to the deviation between PXRD and DSC data related to the presence of crystalline API, the endothermal peak area cannot be considered as a representative value for amorphization of API. The best dosage forms for the P4 and P5 polymers were printed at the same printing conditions, a laser scanning speed of 200 mm/s and a printing temperature of 112.5 °C. Table 5 shows the characteristic comparison of these two batches.

Table 5. Characterization of PVP-VA-based dosage forms from the best performing batches

Batch name	Median mass, mg	N of outliers*	Mass losses, %	API endothermal peak area, mJ
FP4-112.5-200	216.2 ± 5.2	5	4.1	0
FP5-112.5-200	193.6 ± 5.0	2	4.5	0

* - Number of tablets deviate from the average mass by more than 7.5%.

The visual difference of PVP-VA-based dosage forms is presented in Figure 11. The dosage form printed at 75 °C has a shift along the x-y plane and elongation along the z axis, as do the batches printed at 300 and 400 mm/s for P5. The tablets printed at 100 °C and 112.5 °C show the impact of sintering, with those printed at lower laser speeds appearing darker than those printed at higher laser speeds.

Figure 11. PVP-VA-based dosage forms printed at different speeds and temperatures.

Additionally, the crumbly appearance increases, especially at the highest laser scan speed of 400 mm/s, whereas the tablets printed at lower laser scan speeds have denser structures and a shape closer to the designed model. However, the overall appearance of P5-based dosage forms suffers from a number of irregularities and defects for all printing conditions. For instance, the size change for the dosage form printed at 400 mm/s and 100 °C can be seen. Due to poor sintering, the structure starts falling apart, making the shapes irregular and prone to losing drug content. Additionally, the arc-shaped bottom part of batches printed at 200 mm/s is noticeable. This is likely due to the harsh sintering

during the first several layers, which elevates the sintering of the surrounding powder beneath the actual layer.

3.2.3. Effect of polymer selection on SLS 3D printed dosage forms characteristics

The comparison of the printed dosage forms is complicated by the use of several different polymer grades and different print settings. The combination of these two factors has a strong impact on the physical and chemical properties of the final printed dosage forms. PCA was selected to perform a visual comparison of dosage form characteristics representing compliance with Ph. Eur. Therefore, we included the parameters average mass (AM), mass losses (ML) after friability testing, and number of outliers by weight (NO) for evaluation for each batch in this study. The values of these characteristics define the API dosage consistency (AM and NO) and overall dosage form durability (ML), which make them parameters of particular interest with respect to the manufacturing process. Due to the changes in printing temperatures depending on the polymer, the scanning speed was selected as the grouping parameter, as it has the same three values for all printing experiments. The PCA biplot (Figure 12) of all printed batches was acquired in new axes defined by principal components instead of dataset variables. The variables are described by the arrows showing the direction of the most variance. Analyzing the graph, there is an observation of obvious clustering of the printed batches in accordance with scanning speed, which is an indication of the great effect of this parameter on dosage forms characteristics. The batches printed at the highest speed of 400 mm/s are characterized by high friability and high number of outliers, and low average mass. The exception are batches FP1-125-400 and FP2-125-400, which have a low friability value and low numbers of outliers. The batches printed at a speed of 300 mm/s were in the middle with few exceptions; batch FP2-100-300 has a higher friability value and FP3-75-300 has a high number of outliers. The batches printed at a speed of 200 mm/s have the highest average mass and lowest friability and number of outliers. However, the batch FP4-75-200 has one of the highest number of outliers. Moreover, some batches, especially printed at temperatures of 100 and 75 °C are in the overlapping region with a cluster of batches printed at a speed of 300 mm/s.
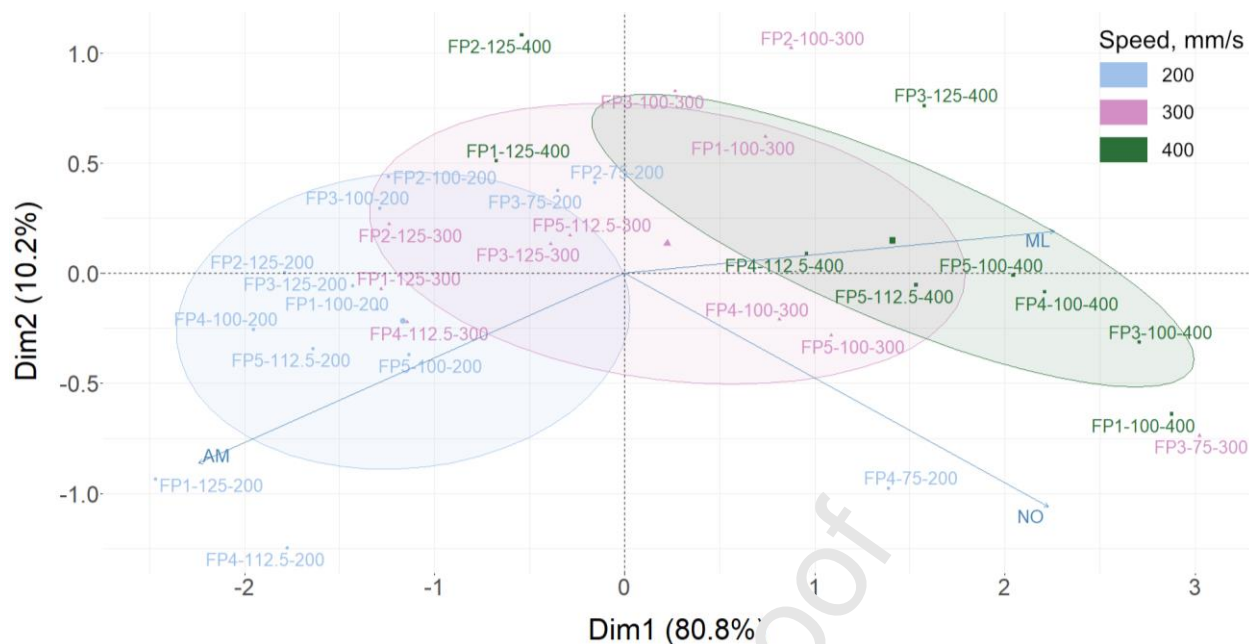
Figure 12. A PCA biplot of printed dosage forms grouped by printing speed.

As shown in the graph, the AM and ML vectors point almost in opposite directions, which is an indication of negative correlation. The higher the average mass, the lower the mass loss. The reason for this correlation is higher energy input for dosage forms printed at lower scanning speed, which provided better sintering and consequently higher average mass and durability. Meanwhile, the angle between AM and NO is close to 90°, which means these two factors are mostly orthogonal, indicating only a small correlation between these factors.

3.3. Drug Content

The drug content of the different dosage forms, which were taken from the best-performing batches according to Ph. Eur. for each different polymer, is presented in Table 7.

Table 7. Drug content for dosage forms with different base polymers.

Batch	FP1-125-200	FP2-125-200	FP3-125-200	FP4-112.5-200	FP5-112.5-200
Drug Loaded (%)	8.6 ± 0.127	8.9 ± 0.301	8.5 ± 0.103	8.5 ± 0.106	8.9 ± 0.170

Each dosage form had a lower drug content than the 10% API theoretical loading. However, all dosage forms had a consistent similar amount of loading, between 8.5-9%. No real trend is observed to differentiate the loading between the PVA-based and PVP-based polymer dosage forms. The difference between theoretical and real drug loading is related to two main factors. First, the powder preparation process includes sieving with a 315 μm sieve, which removes larger particles of API and their agglomerates from the final formulation. Second, there is less binding of API particles by the polymer on the

surface of the dosage forms, which provokes its loss during handling. One noticeable difference was the standard deviation for dosage forms printed with P2, which was higher than for other polymers. All other standard deviations are less than 0.2%, while the standard deviation for P2-based dosage forms is 0.3%, suggesting less uniformity for these dosage forms.

3.4. API dissolution test

According to the PXRD results, the final printed structures might be classified as amorphous solid dispersions (ASDs). These systems are assumed to consist of an amorphous API stabilized by a polymer. One of the main advantages of such binary systems is the enhanced solubility of API.[42]

The dissolution of the different dosage forms, which proceeded with the best-performing batches according to Ph.Eur. for each different polymer, have data shown in Figure 13.

FP1-, FP2-, and FP3-based dosage forms all showed a significant supersaturation of API in the 180 min measurement window. The reason is the amorphization of the API and following formation of ASD in case of using PVA-based polymers, which enhances the solubility. FP1-125-200 showed rapid, quasi-linear, release over time up to 21.8 µg/mL after 180 min, which corresponds to 63.4% of loaded API. Forty times higher supersaturation concentration was achieved after 180 min compared to the pure API. FP3-125-200 follows a visually similar release kinetics as FP1-125-200 for the first 60 min. Then, it reaches a plateau at 120 min with 9.0 µg/mL of released API, which corresponds to 28.6% of loaded API and 17 times higher supersaturation concentration than pure API.

FP2-125-200 also showed a quasi-linear release throughout the measurement window, though lower than that of FP1-125-200 and similar to FP3-125-200 reaching 7.5 µg/mL after 180 min, which corresponds to 24.1% of loaded API and 15 times higher supersaturation concentration than pure API. It has a delayed release, so 1.85 µg/mL of API was released after the first 60 min. The difference in API dissolution profiles for PVA grades can be related to the polymers' different dynamic viscosities (mPa·s) and degree of hydrolyzation (molar %). The dynamic viscosity is a property of the PVA polymer grade, given as the first number of its commercial name. This number represents the dynamic viscosity of a 4% w/v aqueous solution at 20 ˚C. P1 has the lowest dynamic viscosity of 3 mPa·s and highest dissolution rate of API whereas P2 has the highest viscosity of 5 mPa·s and the lowest API dissolution rate. P3, meanwhile, has a viscosity of 4 mPa·s and P3-based dosage forms dissolution rate is between that of P1- and P2-based dosage forms. Hence, the impact of the polymer viscosity on API dissolution rate can be observed, which correlates to data in an earlier published study.[43] The lower the viscosity of the polymer, the higher the dissolution rate of the API. The degree of hydrolysis represents how many of the vinyl acetate units were hydrolyzed. The lower hydrolysis degree provides more remaining acetate groups (hydrophobic) and less hydroxyl groups (hydrophilic) in the structure of the polymer. This combination defines the amphiphilic nature of PVA grades which plays a significant role in the

supersaturated state stabilization.[42] The current study shows that 82% degree of hydrolysis (P1, PVA-3-82) provides the most suitable ratio of acetate and hydroxyl groups for the enhanced solubility of the lipophilic API providing supersaturation concentration 40 times higher than pure API and around 2.5 times higher than other PVA grades. However, there is a noticeable deviation in the cumulative drug release after 180 minutes. This could be due to uneven distribution of the color pigment within the powder, variations in powder reflection properties, temperature gradients, and other related factors during the sintering process. This effect is especially prominent in the case of FP1-125-200. Moreover, it should be noted that PVA tends to swell[41,44], which can potentially lead to deviations in the cumulative release profiles within triplicates. Furthermore, the observed deviation can be attributed to the porous structure of the dosage forms. The presence of pores within the dosage forms can influence the accessibility of the dissolution medium to the API.

It is crucial to note that different PVA grades possess unique combinations of chemical properties. While it was observed that dynamic viscosity predominantly influences the dissolution rate, and no correlation was found between the degree of hydrolysis and dissolution rate, it is worth considering the potential determining impact of the synergistic effect between these two chemical properties.

FP4-125-200 and FP5-125-200, on the other hand, showed an average API release of only 2.01 µg/mL and 1.37 µg/mL after 180 min, respectively. It corresponds to 5.8% and 4.3% of loaded API for FP4-125-200 and FP5-125-200, respectively. Any assumptions regarding PVP-VA grade effect on dissolution rate of API are untenable, due to the high variations within triplicates and the low drug release. Low indomethacin release from SLS printed PVP-VA-based dosage forms has also been shown previously.[45] The average release reached 4.5% after 120 min in a medium of pH 2, which corresponds to data presented in the current study. The inhibition of the API release for PVP-VA-based polymers may be due to the crystalline API residuals shown in PXRD diffractograms. They may act as nucleation centers of API recrystallisation during the dissolution, which decreases the supersaturation concentration. Moreover, the formation of a hydrophobic outer shell upon polymer dissolution may slow down dissolution.[46] Since the API release of PVP-VA dosage forms did not exceed 5 µg/mL, an enlarged version of the dissolution profiles was added to the supplementary information (Figure S11).
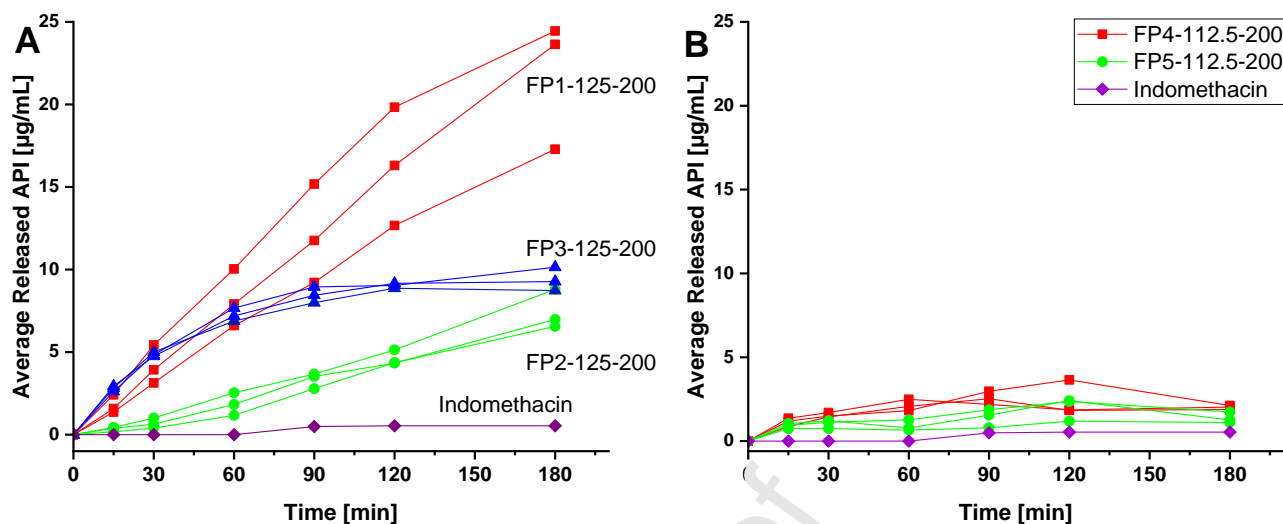
Figure 13. Dissolution profiles of PVA-based (A) and PVP-VA-based (B) dosage forms, as compared to the API, Indomethacin, with average release of API in μg/mL.

Conclusion

The trends seen in this study offer an insight into various grades of polymers that have high potential applicability for SLS produced oral dosage forms. In order for this technology to advance, the properties of the employed materials and their effect on the resultant oral dosage forms must be fully realized, as well as the impact the printing conditions may yield upon the results. Some of the materials used in this study, PVA 3-82 and PVA 5-74, are entirely new, making these results vital for the future applicability and printability of these materials with SLS for pharmaceutical applications. The other materials investigated in this study, while not new on the market, are of high interest for SLS printing, and the results for the printing variations in this study are of importance for printing done with these materials in the future.

In this study, a strong correlation was found for the printing conditions of laser scanning speed and print temperature with regard to the average mass of the resultant dosage forms. In terms of adherence with Ph.Eur., a trend of lower scan speeds and higher temperatures within the ranges of each formulation gave the best print results. When comparing the results of the different grades of materials, PVA-based grades support API amorphization, whereas PVP-VA-based dosage forms have remaining traces of crystallinity. This is particularly reflected in the dissolution results. For the PVA-based dosage forms, a rapid release is observed, while, in case of PVP-VA-based dosage forms, the release is only around 5%. A further finding, when analyzing the dissolution of PVA-based dosage forms, was that a negative correlation between the dynamic viscosity and dissolution rate was observed. The lower the viscosity of these dosage forms, the higher the dissolution rate. Furthermore, the quality of the dosage forms and Ph.Eur. compliance showed correlations with some of the selected polymers. At the same printing conditions, the polymers in the study showed different results. Therefore,

24

the type and grade of the polymer define the suitable printing conditions and, consequently, the tunability of the dosage forms. Using the information gathered in this study, future work on oral dosage form development using SLS could be aided.

Acknowledgements

Evgenii Tikhomirov: Conceptualization, Methodology, Investigation, Writing - original draft, Visualization. **Valerie Levine:** Conceptualization, Methodology, Investigation, Writing - original draft, Visualization. **Michelle Åhlén**: Conceptualization, Methodology, Investigation. **Nicole Di Gallo**: Methodology, Investigation. **Maria Strømme**: Conceptualization, Writing - review & editing, Supervision, Funding acquisition. **Thomas Kipping**: Conceptualization, Writing - review & editing. **Julian Quodbach**: Conceptualization, Writing - review & editing, Supervision. **Jonas Lindh**: Conceptualization, Writing - review & editing, Supervision, Funding acquisition.

Declaration of interests

☐The authors declare that they have no known competing financial interests or personal relationships that could have appeared to influence the work reported in this paper.

☒The authors declare the following financial interests/personal relationships which may be considered as potential competing interests:

References

(1)   Stegemann, S.; Gosch, M.; Breitkreutz, J. Swallowing Dysfunction and Dysphagia Is an Unrecognized Challenge for Oral Drug Therapy. *Int. J. Pharm.* **2012**, *430* (1–2), 197–206. https://doi.org/10.1016/j.ijpharm.2012.04.022.

(2)   Waller, D. G. Off-Label and Unlicensed Prescribing for Children: Have We Made Any Progress? *Br. J. Clin. Pharmacol.* **2007**, *64* (1), 1–2. https://doi.org/10.1111/j.1365-2125.2007.02987.x.

(3)   Liu, F.; Ranmal, S.; Batchelor, H. K.; Orlu-Gul, M.; Ernest, T. B.; Thomas, I. W.; Flanagan, T.; Tuleu, C. Patient-Centered Pharmaceutical Design to Improve Acceptability of Medicines: Similarities and Differences in Paediatric and Geriatric Populations. *Drugs* **2014**, *74* (16), 1871–1889. https://doi.org/10.1007/s40265-014-0297-2.

(4)   Verrue, C.; Mehuys, E.; Boussery, K.; Remon, J.-P.; Petrovic, M. Tablet-Splitting: A Common yet Not so Innocent Practice: Tablet-Splitting. *J. Adv. Nurs.* **2011**, *67* (1), 26–32. https://doi.org/10.1111/j.1365-2648.2010.05477.x.

(5)   van Riet-Nales, D. A.; Doeve, M. E.; Nicia, A. E.; Teerenstra, S.; Notenboom, K.; Hekster, Y. A.; van den Bemt, B. J. F. The Accuracy, Precision and Sustainability of Different Techniques for Tablet Subdivision: Breaking by Hand and the Use of Tablet Splitters or a Kitchen Knife. *Int. J. Pharm.* **2014**, *466* (1–2), 44–51. https://doi.org/10.1016/j.ijpharm.2014.02.031.

(6)   Walsh, J.; Ranmal, S. R.; Ernest, T. B.; Liu, F. Patient Acceptability, Safety and Access: A Balancing Act for Selecting Age-Appropriate Oral Dosage Forms for Paediatric and Geriatric Populations. *Int. J. Pharm.* **2018**, *536* (2), 547–562. https://doi.org/10.1016/j.ijpharm.2017.07.017.

(7)   Windolf, H.; Chamberlain, R.; Quodbach, J. Predicting Drug Release from 3D Printed Oral Medicines Based on the Surface Area to Volume Ratio of Tablet Geometry. *Pharmaceutics* **2021**, *13* (9), 1453. https://doi.org/10.3390/pharmaceutics13091453.

(8)   Cailleaux, S.; Sanchez-Ballester, N. M.; Gueche, Y. A.; Bataille, B.; Soulairol, I. Fused Deposition Modeling (FDM), the New Asset for the Production of Tailored

Medicines. *J. Controlled Release* **2021**, *330*, 821–841.
https://doi.org/10.1016/j.jconrel.2020.10.056.

(9)   Araújo, M.; Sa-Barreto, L.; Gratieri, T.; Gelfuso, G.; Cunha-Filho, M. The Digital Pharmacies Era: How 3D Printing Technology Using Fused Deposition Modeling Can Become a Reality. *Pharmaceutics* **2019**, *11* (3), 128.
https://doi.org/10.3390/pharmaceutics11030128.

(10)   Gibson, I.; Rosen, D.; Stucker, B. *Additive Manufacturing Technologies*; Springer New York: New York, NY, 2015. https://doi.org/10.1007/978-1-4939-2113-3.

(11)   Wang, Z.; Han, X.; Chen, R.; Li, J.; Gao, J.; Zhang, H.; Liu, N.; Gao, X.; Zheng, A. Innovative Color Jet 3D Printing of Levetiracetam Personalized Paediatric Preparations. *Asian J. Pharm. Sci.* **2021**, *16* (3), 374–386.
https://doi.org/10.1016/j.ajps.2021.02.003.

(12)   Wilts, E. M.; Long, T. E. Sustainable Additive Manufacturing: Predicting Binder Jettability of Water-soluble , Biodegradable and Recyclable Polymers. *Polym. Int.* **2021**, *70* (7), 958–963. https://doi.org/10.1002/pi.6108.

(13)   Sen, K.; Mehta, T.; Sansare, S.; Sharifi, L.; Ma, A. W. K.; Chaudhuri, B. Pharmaceutical Applications of Powder-Based Binder Jet 3D Printing Process – A Review. *Adv. Drug Deliv. Rev.* **2021**, *177*, 113943.
https://doi.org/10.1016/j.addr.2021.113943.

(14)   Kozakiewicz-Latała, M.; Nartowki, K. P.; Dominik, A.; Malec, K.; Gołkowska, A. M.; Złocińska, A.; Rusińska, M.; Szymczyk-Ziółkowska, P.; Ziółkowski, G.; Górniak, A.; Karolewicz, B. Binder Jetting 3D Printing of Challenging Medicines: From Low Dose Tablets to Hydrophobic Molecules. *Eur. J. Pharm. Biopharm.* **2022**, *170*, 144–159. https://doi.org/10.1016/j.ejpb.2021.11.001.

(15)   Karalia, D.; Siamidi, A.; Karalis, V.; Vlachou, M. 3D-Printed Oral Dosage Forms: Mechanical Properties, Computational Approaches and Applications. *Pharmaceutics* **2021**, *13* (9), 1401. https://doi.org/10.3390/pharmaceutics13091401.

(16)   Carl R. Deckard. Method and Apparatus for Producing Parts by Selective Sintering. 4,863,538, September 5, 1989.

(17)   Fina, F.; Goyanes, A.; Gaisford, S.; Basit, A. W. Selective Laser Sintering (SLS) 3D Printing of Medicines. *Int. J. Pharm.* **2017**, *529* (1), 285–293.
https://doi.org/10.1016/j.ijpharm.2017.06.082.

(18)   Niu, H. J.; Chang, I. T. H. Selective Laser Sintering of Gas Atomized M2 High Speed Steel Powder. *J. Mater. Sci.* **2000**, *35* (1), 31–38.
https://doi.org/10.1023/A:1004720011671.

(19)   Kumar, S. Selective Laser Sintering: A Qualitative and Objective Approach. *JOM* **2003**, *55* (10), 43–47. https://doi.org/10.1007/s11837-003-0175-y.

(20)   Manthiram, A.; Bourell, D. L.; Marcus, H. L. Nanophase Materials in Solid Freeform Fabrication. *JOM* **1993**, *45* (11), 66–70. https://doi.org/10.1007/BF03222493.

(21)   Sing, S. L.; Yeong, W. Y.; Wiria, F. E.; Tay, B. Y.; Zhao, Z.; Zhao, L.; Tian, Z.; Yang, S. Direct Selective Laser Sintering and Melting of Ceramics: A Review. *Rapid Prototyp. J.* **2017**, *23* (3), 611–623. https://doi.org/10.1108/RPJ-11-2015-0178.

(22)   Chen, A.-N.; Wu, J.-M.; Liu, K.; Chen, J.-Y.; Xiao, H.; Chen, P.; Li, C.-H.; Shi, Y.-S. High-Performance Ceramic Parts with Complex Shape Prepared by Selective Laser Sintering: A Review. *Adv. Appl. Ceram.* **2018**, *117* (2), 100–117. https://doi.org/10.1080/17436753.2017.1379586.

(23)   Wu, B. M.; Borland, S. W.; Giordano, R. A.; Cima, L. G.; Sachs, E. M.; Cima, M. J. Solid Free-Form Fabrication of Drug Delivery Devices. *J. Controlled Release* **1996**, *40* (1–2), 77–87. https://doi.org/10.1016/0168-3659(95)00173-5.

(24)   Trenfield, S. J.; Xu, X.; Goyanes, A.; Rowland, M.; Wilsdon, D.; Gaisford, S.; Basit, A. W. Releasing Fast and Slow: Non-Destructive Prediction of Density and Drug Release from SLS 3D Printed Tablets Using NIR Spectroscopy. *Int. J. Pharm. X* **2023**, *5*, 100148. https://doi.org/10.1016/j.ijpx.2022.100148.

(25)   Gueche, Y. A.; Sanchez-Ballester, N. M.; Cailleaux, S.; Bataille, B.; Soulairol, I. Selective Laser Sintering (SLS), a New Chapter in the Production of Solid Oral Forms (SOFs) by 3D Printing. *Pharmaceutics* **2021**, *13* (8), 1212. https://doi.org/10.3390/pharmaceutics13081212.

(26)   Abdalla, Y.; Elbadawi, M.; Ji, M.; Alkahtani, M.; Awad, A.; Orlu, M.; Gaisford, S.; Basit, A. W. Machine Learning Using Multi-Modal Data Predicts the Production of Selective Laser Sintered 3D Printed Drug Products. *Int. J. Pharm.* **2023**, *633*, 122628. https://doi.org/10.1016/j.ijpharm.2023.122628.

(27)   Thakkar, R.; Thakkar, R.; Pillai, A.; Ashour, E. A.; Repka, M. A. Systematic Screening of Pharmaceutical Polymers for Hot Melt Extrusion Processing: A Comprehensive Review. *Int. J. Pharm.* **2020**, *576*, 118989. https://doi.org/10.1016/j.ijpharm.2019.118989.

(28)   Maniruzzaman, M.; Boateng, J. S.; Snowden, M. J.; Douroumis, D. A Review of Hot-Melt Extrusion: Process Technology to Pharmaceutical Products. *ISRN Pharm.* **2012**, *2012*, 1–9. https://doi.org/10.5402/2012/436763.

(29)   Tabriz, A. G.; Scoutaris, N.; Gong, Y.; Hui, H.-W.; Kumar, S.; Douroumis, D. Investigation on Hot Melt Extrusion and Prediction on 3D Printability of Pharmaceutical Grade Polymers. *Int. J. Pharm.* **2021**, *604*, 120755. https://doi.org/10.1016/j.ijpharm.2021.120755.

(30)   Hwang, I.; Kang, C.-Y.; Park, J.-B. Advances in Hot-Melt Extrusion Technology toward Pharmaceutical Objectives. *J. Pharm. Investig.* **2017**, *47* (2), 123–132. https://doi.org/10.1007/s40005-017-0309-9.

(31)   *Parteck® MXP Excipient for Hot Melt Extrusion | Small Molecule Pharmaceuticals | Merck*. https://www.merckmillipore.com/SE/en/products/small-molecule-pharmaceuticals/formulation/solid-dosage-form/parteck-excipients/parteck-mxp/Ieyb.qB.lAcAAAFYLEQeWww_,nav?ReferrerURL=https%3A%2F%2Fwww.google.com%2F (accessed 2022-12-14).

(32)   Samaro, A.; Janssens, P.; Vanhoorne, V.; Van Renterghem, J.; Eeckhout, M.; Cardon, L.; De Beer, T.; Vervaet, C. Screening of Pharmaceutical Polymers for Extrusion-Based Additive Manufacturing of Patient-Tailored Tablets. *Int. J. Pharm.* **2020**, *586*, 119591. https://doi.org/10.1016/j.ijpharm.2020.119591.

(33)   Yang, Y.; Xu, Y.; Wei, S.; Shan, W. Oral Preparations with Tunable Dissolution Behavior Based on Selective Laser Sintering Technique. *Int. J. Pharm.* **2021**, *593*, 120127. https://doi.org/10.1016/j.ijpharm.2020.120127.

(34)   *Merck Launches Parteck® MXP Excipient for Increased Solubility*. https://www.merckgroup.com/en/news/parteck-02-12-2016.html (accessed 2022-12-14).

(35)   *Kollidon® VA 64 | Povidones, Copovidones, Crospovidones*. BASF Pharma. https://pharma.basf.com/products/kollidon-va-64 (accessed 2022-12-15).

(36)   Gueche, Y. A.; Sanchez-Ballester, N. M.; Bataille, B.; Aubert, A.; Rossi, J.-C.; Soulairol, I. A QbD Approach for Evaluating the Effect of Selective Laser Sintering Parameters on Printability and Properties of Solid Oral Forms. *Pharmaceutics* **2021**, *13* (10), 1701. https://doi.org/10.3390/pharmaceutics13101701.

(37)   Kolter, K.; Karl, M.; Gryczke, A. *Hot-Melt Extrusion with BASF Pharma Polymers: Extrusion Compendium*, 2nd revised and enlarged edition.; BASF: Ludwigshafen, 2012.

(38)   *European Pharmacopoeia*, 10th ed.; C.o. Europe: Strasbourg, 2020.

(39)   Kruth, J.-P.; Mercelis, P.; Van Vaerenbergh, J.; Froyen, L.; Rombouts, M. Binding Mechanisms in Selective Laser Sintering and Selective Laser Melting. https://doi.org/10.1108/13552540510573365.

(40)   Hassan, C. M.; Peppas, N. A. Structure and Applications of Poly(Vinyl Alcohol) Hydrogels Produced by Conventional Crosslinking or by Freezing/Thawing Methods. In *Biopolymers · PVA Hydrogels, Anionic Polymerisation Nanocomposites*; Advances in Polymer Science; Springer Berlin Heidelberg: Berlin, Heidelberg, 2000; Vol. 153, pp 37–65. https://doi.org/10.1007/3-540-46414-X_2.

(41)   Tikhomirov, E.; Åhlén, M.; Di Gallo, N.; Strømme, M.; Kipping, T.; Quodbach, J.; Lindh, J. Selective Laser Sintering Additive Manufacturing of Dosage Forms: Effect of Powder Formulation and Process Parameters on the Physical Properties of Printed Tablets. *Int. J. Pharm.* **2023**, *635*, 122780. https://doi.org/10.1016/j.ijpharm.2023.122780.

(42)   Wlodarski, K.; Zhang, F.; Liu, T.; Sawicki, W.; Kipping, T. Synergistic Effect of Polyvinyl Alcohol and Copovidone in Itraconazole Amorphous Solid Dispersions. *Pharm. Res.* **2018**, *35* (1), 16. https://doi.org/10.1007/s11095-017-2313-1.

(43)   Shi, N.-Q.; Jin, Y.; Zhang, Y.; Che, X.-X.; Xiao, X.; Cui, G.-H.; Chen, Y.-Z.; Feng, B.; Li, Z.-Q.; Qi, X.-R. The Influence of Cellulosic Polymer's Variables on Dissolution/Solubility of Amorphous Felodipine and Crystallization Inhibition from a Supersaturated State. *AAPS PharmSciTech* **2019**, *20* (1), 12. https://doi.org/10.1208/s12249-018-1266-y.

(44)   LaFountaine, J. S.; Jermain, S. V.; Prasad, L. K.; Brough, C.; Miller, D. A.; Lubda, D.; McGinity, J. W.; Williams, R. O. Enabling Thermal Processing of Ritonavir–Polyvinyl Alcohol Amorphous Solid Dispersions by KinetiSol® Dispersing. *Eur. J. Pharm. Biopharm.* **2016**, *101*, 72–81. https://doi.org/10.1016/j.ejpb.2016.01.018.

(45)   Thakkar, R.; Zhang, Y.; Zhang, J.; Maniruzzaman, M. Synergistic Application of Twin-Screw Granulation and Selective Laser Sintering 3D Printing for the Development of Pharmaceutical Dosage Forms with Enhanced Dissolution Rates and Physical

Properties. *Eur. J. Pharm. Biopharm.* **2021**, *163*, 141–156.
https://doi.org/10.1016/j.ejpb.2021.03.016.

(46)   Tres, F.; Treacher, K.; Booth, J.; Hughes, L. P.; Wren, S. A. C.; Aylott, J. W.; Burley, J. C. Indomethacin-Kollidon VA64 Extrudates: A Mechanistic Study of PH-Dependent Controlled Release. *Mol. Pharm.* **2016**, *13* (3), 1166–1175.
https://doi.org/10.1021/acs.molpharmaceut.5b00979.